JACS
JOURNAL OF THE AMERICAN CHEMICAL SOCIETY
Article
pubs.acs.org/JACS

Linker Installation: Engineering Pore Environment with Precisely Placed Functionalities in Zirconium MOFs

Shuai Yuan,[†,⊥] Ying-Pin Chen,[†,‡,⊥] Jun-Sheng Qin,[†] Weigang Lu,[§] Lanfang Zou,[†] Qiang Zhang,[†] Xuan Wang,[†] Xing Sun,[†,‡] and Hong-Cai Zhou*[,†,‡]

[†]Department of Chemistry, Texas A&M University, College Station, Texas 77843-3255, United States
[‡]Department of Materials Science and Engineering, Texas A&M University, College Station, Texas 77842, United States
[§]Department of Chemistry, Blinn College, Bryan, Texas 77805, United States

Supporting Information

ABSTRACT: Precise placement of multiple functional groups in a highly ordered metal−organic framework (MOF) platform allows the tailoring of the pore environment, which is required for advanced applications. To realize this, we present a comprehensive study on the linker installation method, in which a stable MOF with coordinatively unsaturated Zr_6 clusters was employed and linkers bearing different functional groups were postsynthetically installed. A Zr-MOF with inherent missing linker sites, namely, PCN-700, was initially constructed under kinetic control. Twelve linkers with different substituents were then designed to study their effect on MOF formation kinetics and therefore resulting MOF structures. Guided by the geometrical analysis, linkers with different lengths were installed into a parent PCN-700, giving rise to 11 new MOFs and each bearing up to three different functional groups in predefined positions. Systematic variation of the pore volume and decoration of pore environment were realized by linker installation, which resulted in synergistic effects including an enhancement of H_2 adsorption capacities of up to 57%. In addition, a size-selective catalytic system for aerobic alcohol oxidation reaction is built in PCN-700 through linker installation, which shows high activity and tunable size selectivity. Altogether, these results exemplify the capability of the linker installation method in the pore environment engineering of stable MOFs with multiple functional groups, giving an unparalleled level of control.

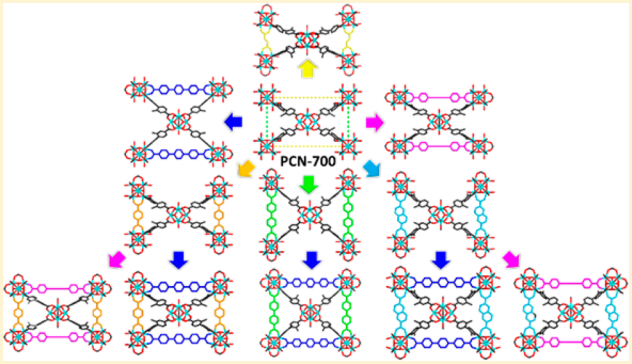

INTRODUCTION

As a new emerging class of highly ordered porous materials, metal−organic frameworks (MOFs) have attracted great attention in the last two decades.[1] Their modular nature imparts designable topology, adjustable porosity, tunable functionality, and variable surface moieties within a single material,[2] which have potential applications in many areas including gas storage, separation, and catalysis.[3] Among the known MOF materials, Zr-based MOFs have been intensively studied because of their superior stability against moist atmosphere, aqueous solutions, as well as basic or acidic media.[4] The robustness arising from the kinetic inertness of the Zr−carboxylate bonds enables advanced applications in MOF systems. However, the synthesis of Zr-MOF usually requires elevated temperature and high concentration of acids as modulating reagents.[5] Such harsh conditions can prohibit labile and reactive functional groups from being incorporated into Zr-MOFs in a one-pot reaction, thus limiting the functionalization of the Zr-MOFs for further exploitation.[6]

To address this issue, postsynthetic modification methods have been successfully employed to introduce functionalities to Zr-MOFs under relatively mild conditions.[7] Cohen and co-workers demonstrated that labile diiron complexes as hydrogen generation catalysts can be incorporated into a Zr-MOF, UiO-66, via postsynthetic linker exchange.[8] The Hupp group developed a solvent-assisted ligand incorporation strategy to introduce terminal carboxylate or phosphate ligands on Zr_6 clusters.[9] Our group has shown that various functional groups with controlled loading can be anchored onto linkers of Zr-MOFs via a click reaction, endowing the MOFs with tailored interfaces.[10] However, it is still difficult to include multiple functional groups simultaneously in a MOF pore. Additionally, the reported postsynthetic modification methods of Zr-MOFs typically lack a high level of control over the distribution of the incorporated functionalities. Placing multiple functionalities with synergistic effects in a MOF cavity is particularly interesting for many potential applications.[11] For example, programmed pore architectures are realized in a MUF-7 system, which is constructed from Zn_4O clusters and three linkers with different lengths or symmetries.[12] This prompts us to develop stepwise synthetic routes to sequentially introduce function-

Received: May 2, 2016
Published: June 25, 2016

DOI: 10.1021/jacs.6b04501
J. Am. Chem. Soc. 2016, 138, 8912−8919

alities in robust Zr-MOFs and therefore control their positions and distributions.

Our group has reported a new method, linker installation, to precisely place different functionalities into Zr-MOFs under mild conditions.[13] In this method, a Zr-MOF constructed from 8-connected $Zr_6O_4(OH)_8(H_2O)_4$ clusters was selected as a matrix. Linear carboxylate linkers with various functionalities were postsynthetically installed into the matrix by replacing the terminal OH^-/H_2O ligands of adjacent $Zr_6O_4(OH)_8(H_2O)_4$ clusters.[9d,14] Since linkers with different lengths were installed in predesigned positions in the MOF structure, multiple functional groups were therefore precisely placed at defined locations in the MOF cavity. In our previous work, we demonstrated that two linkers with different functional groups can be sequentially installed into a Zr-MOF.[13] Herein, we perform a comprehensive study on the linker installation method. First, a MOF with predesigned missing linker sites, namely, PCN-700, was synthesized under kinetic control. Twelve linkers with different substituents were designed to study the effect of substituents on MOF structures. Guided by geometrical analysis, 11 different mixed-linker MOFs were derived from PCN-700 by linker installation, each bearing up to three different functional groups in predefined positions. Systematic variation of pore volume and decoration of pore environment were realized by linker installation, which resulted in an enhancement of H_2 adsorption capacities of up to 57%. At last, a size-selective catalytic system for aerobic alcohol oxidation was built in PCN-700 by sequential installation of BPYDC(Cu) (BPYDC = 2,2′-bipyridine-5,5′-dicarboxylate) and TPDC-R_2 (TPDC = terphenyl-4,4″-dicarboxylate, R = Me, Ph, or Hex). In light of the ubiquity of Zr-MOFs with reduced connectivity, we believe that linker installation is a versatile strategy to precisely place functionalities within robust MOF platforms under mild conditions.

RESULTS AND DISCUSSION

Controlling MOF Structure by Linker Design. It is known that the substituents on MOF linkers could affect the conformation of linkers, which in turn changes the vertex geometry, structure dimensionality, and topology of resulting frameworks.[4e,15] In our previous work, we showed that by introducing two methyl groups at the 2- and 2′-positions of BPDC (biphenyl-4,4′-dicarboxylate), a Zr-MOF with **bcu** topology can be synthesized, namely, PCN-700.[13] In distinct contrast to UiO-type structures with **fcu** topology and 12-connected $Zr_6O_4(OH)_4$ clusters,[4a] PCN-700 is a **bcu** net constructed from 8-connected $Zr_6O_4(OH)_8(H_2O)_4$ clusters.

A challenge encountered in the synthesis of PCN-700 is the formation of competing phases, known as the UiO structures, with the desired PCN-700 product. When combined with linear linkers such as BPDC, Zr_6 clusters can form an **fcu** net (UiO-67 structure, Figure 1c,e) or a **bcu** net (PCN-700 structure, Figure 1d,f) depending on the conformation of linkers. In the **fcu** net, two carboxylates of each linker adopt a coplanar conformation (Figure 1a), whereas the two carboxylates are perpendicular to each other in the **bcu** net (Figure 1b). Considering the fact that the formation of the Zr−carboxylate bond is an exothermic process, the **fcu** net, with 12-connected Zr_6 clusters, is believed to be thermodynamically more favorable than the 8-connected **bcu** net.[16] However, the coplanar conformation is kinetically unfavorable if bulky substituents are introduced on the 2- and 2′-positions of BPDC. The steric hindrance of substituents will force the two phenyl rings as well as the carboxylates into a

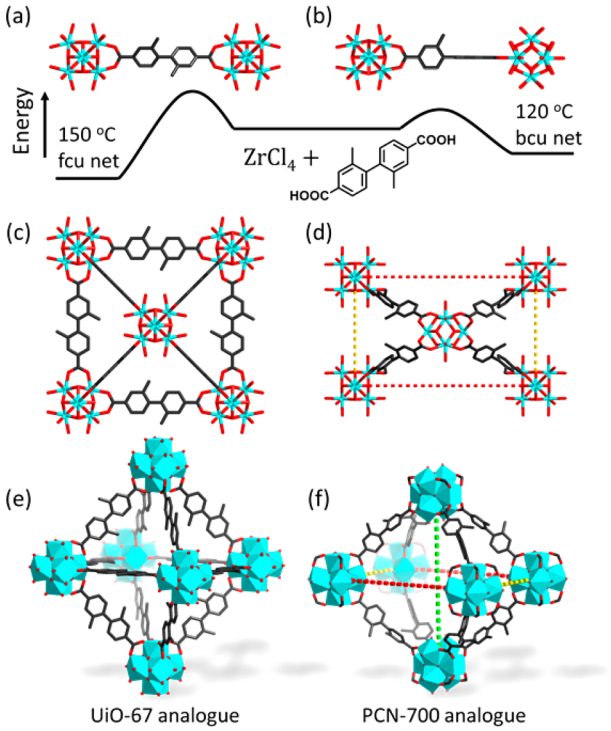

Figure 1. Kinetic control in the synthesis of PCN-700: (a) linker conformation in **fcu** nets; (b) linker conformation in **bcu** nets; (c) UiO-67 and (d) PCN-700 structures viewed along the *a*-axis; cages of (e) UiO-67 and (f) PCN-700 structures.

perpendicular arrangement (Figure 1b), which would increase the energy barrier of **fcu** nets formation because the two carboxylates are required to be coplanar (Figure 1a). Therefore, we assume that a **bcu** net could be obtained as a kinetically controlled product if bulky substituents are introduced on the phenyl rings of the linkers. The competitive formation of the UiO-67 structure and PCN-700 structure represents the competition between thermodynamics and kinetics.

To verify our hypothesis, 12 linkers with different substituents (L1−L12, Scheme 1) were synthesized and reacted

Scheme 1. Linkers with Different Substituents Used in This Work

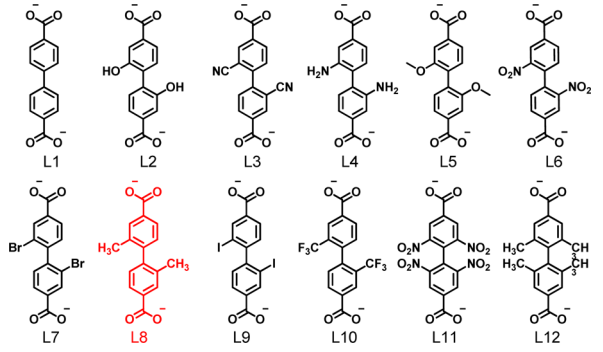

with $ZrCl_4$ at different temperatures. The products were characterized by powder X-ray diffraction and compared with the simulated patterns of UiO-67 and PCN-700. As shown in Figure 2, a phase diagram can be summarized to describe the products from different linkers under variable temperatures. As expected, the resulting MOF structures are strongly dependent

DOI: 10.1021/jacs.6b04501
J. Am. Chem. Soc. 2016, 138, 8912−8919

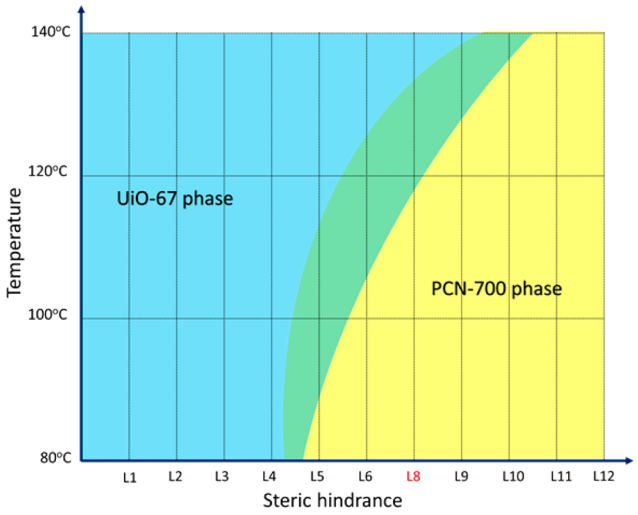

Figure 2. Phase diagram showing the products with different linkers under different temperatures.

on the level of steric hindrance and the number of substituents. In general, PCN-700 is the dominant phase if bulky substituents are introduced on the linkers. Empirically, the steric hindrance of substituents on each linker needs to be larger than that of L5 in order to form PCN-700 isostructures. It should be noted that the "steric argument" cannot explain all the experimental results. As long as steric effect is concerned, L7 is more likely to give the PCN-700 structure than L5 considering that the bromo group is bulkier than the methoxy group. However, the employment of L5 gave rise to the PCN-700 structure, whereas L7 only resulted in the UiO-67 structure under identical synthetic conditions. This is tentatively attributed to the stronger interaction between methoxy groups, which favors the perpendicular conformation. Therefore, L7 does not fit in the phase diagram. Meanwhile, the temperature also affects the final products as it controls the balance between kinetic and thermodynamic products. The PCN-700 phase, as a kinetic product, is favored at relatively low temperature. For example, the L6 would give rise to a pure PCN-700 phase at 80 and 100 °C, whereas a mixture of UiO-67 and PCN-700 phases would be generated if the reaction is carried out at 120 °C. When the reaction temperature is further elevated to 140 °C, only the UiO-67 phase can be obtained. Therefore, pure PCN-700 isostructural product can be synthesized by the rational design of the linkers and judicious control of reaction conditions, which steers the system toward the PCN-700 phases and away from the competing UiO-67 phases.

The L8 linker was selected from 12 linkers to construct the matrix for linker installation studies. Obviously, L1−L5 and L7 are not suitable for linker installation purposes as they tend to form UiO-67 phases under solvothermal conditions. L6 gave rise to a pure PCN-700 phase at 100 °C with low yield. Intuitively, L9−L12 would be adequate for linker installation studies as they form the PCN-700 phase at a wide range of temperatures. However, it should be noted that increasing the steric hindrance of substituents on the linker will decrease the MOF porosity and flexibility as proven by N_2 adsorption studies (Figure S17). Obviously, a rigid and less porous structure is not suitable for the installation of different linkers. The structure constructed from L8 possesses a delicate balance between enough steric effects and sufficient space. Hence, L8 was chosen as a representative example for the further investigation of linker installation.

Geometrical Prediction of Linker Installation. Previously, we demonstrated that BDC (1,4-benzenedicarboxylate) and TPDC-Me_2 can be sequentially installed into PCN-700 by replacing terminal OH^-/H_2O ligands through an acid−base reaction.[13] The PCN-700 structure shows a high degree of flexibility, which can adapt to the postsynthetically installed linkers. This inspires us to explore other possible combinations of linear linkers that can be installed into PCN-700.

Geometrical analysis is used to predict the possible combinations. A cage is taken from PCN-700 and simplified as an octahedron (Figure 3a). There are three pockets in each

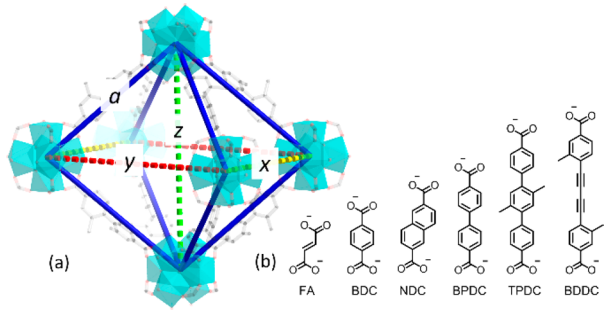

Figure 3. (a) Illustration of the octahedral cage in PCN-700; (b) linear linkers used for linker installation.

cage for accommodation of linear linkers, the lengths of which are denoted as x, y, and z. The length of the original linker L8 in PCN-700, denoted as α, can be measured directly from the single-crystal structure. For simplicity, the above lengths are obtained by measuring the distance between the centers of adjacent clusters. The length α is a constant (α = 18.9 Å), while x, y, and z are variables. An equation can be deduced from the geometrical calculation, which describes the relationship between α, x, y, and z (eq 1).

$$4\alpha^2 = x^2 + y^2 + z^2 \quad (1)$$

By solving this equation, we are able to predict possible combinations of linkers that can be installed into PCN-700. Mathematically, there are infinite solutions for a ternary quadric equation. In reality, however, the length of x, y, and z are limited by existing organic linkers. Considering the size of pockets in PCN-700, six linear linkers with different lengths were selected (Figure 3b), namely, FA (fumarate), BDC, NDC (2,6-napthalenedicarboxylate), BPDC, TPDC, and BDDC (4,4′-(1,3-butadiyne-1,4-diyl)bis(3-methylbenzoate)). When this was taken into consideration, 11 combinations of these linkers can be installed into PCN-700 according to eq 1, which are summarized in Table 1.

To prove our prediction, the linker installation process was carried out by soaking PCN-700 crystals in the solution of linear linkers at 75 °C for 24 h. The afforded crystals were washed with fresh DMF before single-crystal X-ray diffraction data collection. Single-crystal to single-crystal transformation was realized; hence, the positions of subsequently installed linkers were unambiguously observed in the crystallographically resolved structure (Figures 4, S2, and S3). All of the predicted MOFs were experimentally obtained and confirmed by single-crystal X-ray diffraction and powder X-ray diffraction analysis (Figures S4−S15). The pristine PCN-700 structure crystallizes

DOI: 10.1021/jacs.6b04501
J. Am. Chem. Soc. 2016, 138, 8912−8919

Table 1. Geometrically Predicted Combinations of Linkers That Could Be Installed in PCN-700

	length (Å)										
number	1	2	3	4	5	6	7	8	9	10	11
x	**9.1**	**15.4**	**16.8**	**18.9**	19.0	15.7	**15.4**	**15.4**	**16.8**	**16.8**	**18.9**
y	25.9	24.4	23.9	23.1	**23.1**	**24.3**	**23.1**	**24.4**	**23.1**	**24.0**	**23.1**
z	25.9	24.4	23.9	23.1	**23.1**	**24.3**	25.6	**24.4**	24.8	**24.0**	**23.1**
x	FA	BDC	NDC	BPDC			BDC	BDC	NDC	NDC	BPDC
y					TPDC	BDDC	TPDC	BDDC	TPDC	BDDC	TPDC
z					TPDC	BDDC		BDDC		BDDC	TPDC

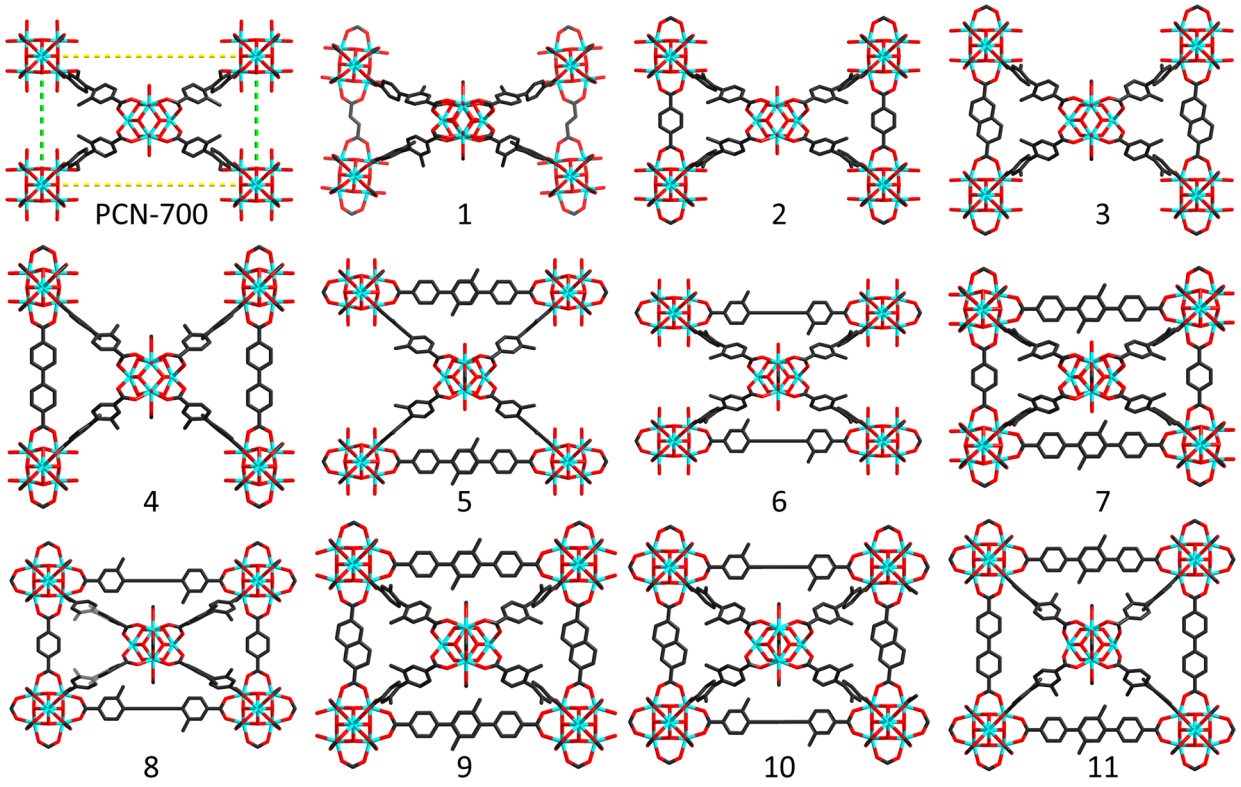

Figure 4. Single-crystal structures of 11 geometrically predicted MOFs resulting from linker installation of PCN-700 viewed along the *a*-axis.

in a tetragonal crystal system with the $P4_2/mmc$ space group. Each $Zr_6O_4(OH)_8(H_2O)_4$ cluster is connected to eight L8 linkers, giving rise to a **bcu** net. Compounds **1**−**6** are formed by installation of FA, NDC, BDC, BPDC, TPDC, and BDDC into PCN-700, respectively, which contains two different linear linkers and 10-connected $Zr_6O_4(OH)_6(H_2O)_2$ clusters. Those MOFs are formulated as $Zr_6O_4(OH)_6(H_2O)_2(L8)_4L$ (L = FA, BDC, BPDC, TPDC, or BDDC), and their structures can be simplified as **bct** nets.

Sequential treatment of PCN-700 crystals with different linkers of appropriate lengths leads to the installation of two linkers. For example, installation of BPDC to PCN-700 gives rise to compound **3**, which can further transform into compound **11** when treated with TPDC solution. Compounds **7**−**11** are composed of three different linear linkers, including one pristine linker from the framework and two postsynthetically inserted ones. They can be classified into two groups depending on the connection number of Zr_6 clusters. Compounds **7** and **9** contain 11-connected $Zr_6O_4(OH)_5(H_2O)$ clusters and possess **ela** topology. Their overall compositions can be formulated as $Zr_6O_4(OH)_5(H_2O)(L8)_4LL'_{0.5}$ (L = BDC or NDC; L′ = TPDC). In these compounds, two pockets are occupied in an octahedral cage, leaving one pocket empty. The size of the unoccupied pocket does not match with any linkers, thus no linker is installed during the treatment. Compounds **8**, **10**, and **11** containing 12-connected $Zr_6O_4(OH)_4$ clusters can be formulated as $Zr_6O_4(OH)_4(L8)_4LL'$ (L = BDC, NDC, or BPDC; L′ = TPDC or BDDC). The overall structure can be simplified into a 12-connected net with a point symbol of $\{3^{24}\cdot 4^{28}\cdot 5^{13}\cdot 6\}$.[17] In these compounds, the size of two linkers perfectly matches with the size of pockets in PCN-700 so that all the pockets in the octahedral cage are occupied. Mathematically, the size of the linkers in compounds **8**, **10**, and **11** satisfy eq 1 and $y = z$ simultaneously. The composition of compound **1** to **11** was determined by single-crystal X-ray diffractions and confirmed by ^{1}H NMR of digested samples (Figures S21−S29 and Table S3). Linker installation is necessary for the synthesis of compounds **1**−**11**. We attempted to synthesize mixed-linker Zr-MOFs starting from a combination of L8 and other linear linkers through a one-pot synthetic approach; however, a mixture of PCN-700 and UiO phases are usually obtained. In the one-pot synthesis, the competitive formation of different products makes it exceedingly challenging to achieve mixed-linker MOFs.

DOI: 10.1021/jacs.6b04501
J. Am. Chem. Soc. 2016, 138, 8912−8919

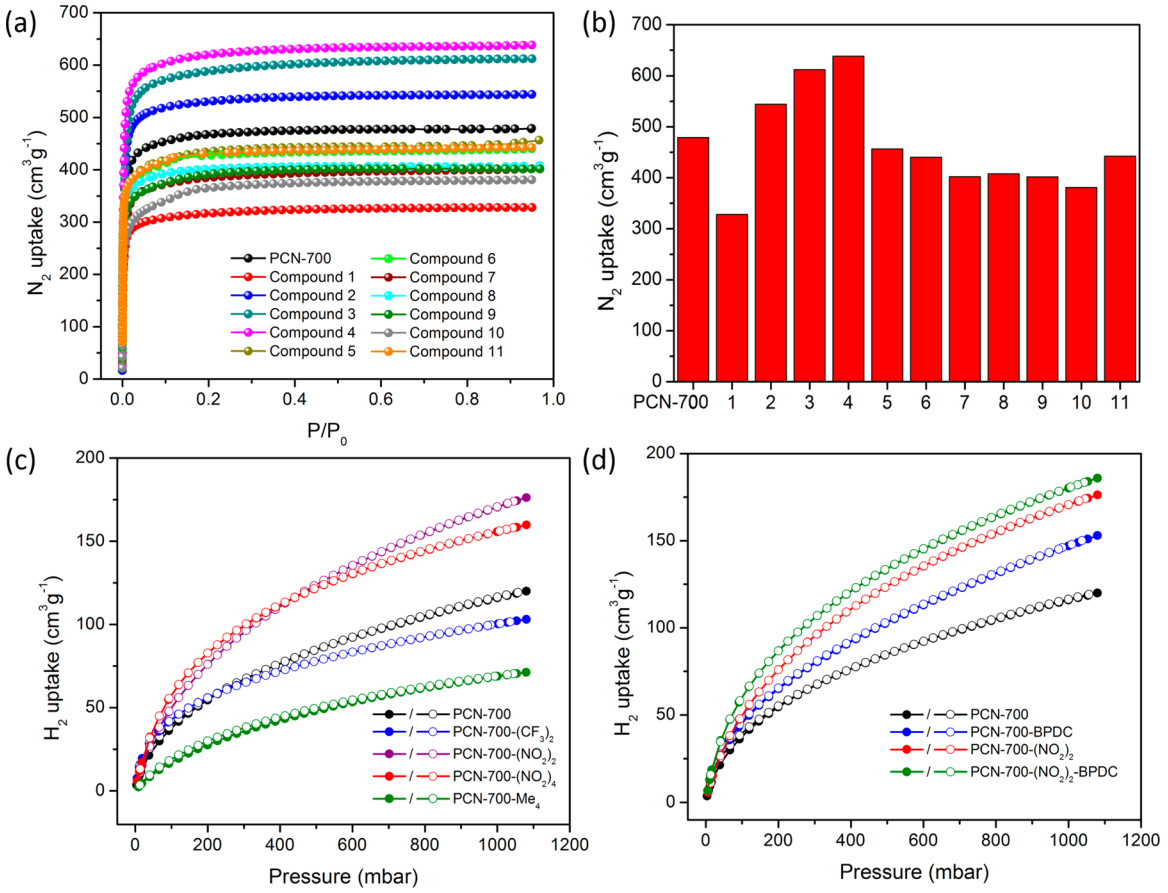

Figure 5. (a) N_2 adsorption isotherms of PCN-700 and compounds **1**−**11** at 77 K. (b) Comparison of total N_2 uptake of PCN-700 and compounds **1**−**11**, demonstrating the control of pore volume by linker installation. (c) H_2 adsorption−desorption isotherms of PCN-700 decorated with different functional groups at 77 K. (d) H_2 adsorption−desorption isotherms of PCN-700 with different functional groups and installed linkers at 77 K showing the synergistic effect of linker installation and linker functionalization.

The flexibility of PCN-700 plays an important role in linker installation. The unit cell parameters along the *c*-axis vary from 11.8 to 19.1 Å in different compounds, allowing for structural adaptation corresponding to the installed linkers. The installed linkers also possess certain flexibility, which ensures the successful installation of linkers even though their lengths do not strictly match the calculation. For example, the lengths of BDDC are 16.4 and 16.1 Å in compounds **7** and **10**, respectively, so that BDDC can pair with both BDC and NDC. In light of the ubiquity of the linker installation method, a variety of promising applications can be envisioned in the PCN-700 platform.

Engineering the Pore Environment by Linker Installation. Linker installation is a unique strategy to control the MOF porosity by incorporation of different linkers. The installed linkers affect the shape and size of MOF cavities, which in turn influence their sorption properties. Furthermore, linkers can be precisely placed at determined channels within the crystalline lattice, and thus the opening and closing of each cavity can be readily controlled. Consequently, an engineered pore architecture can be realized.[12]

The N_2 adsorption measurements were carried out for PCN-700 and compounds **1**−**11** in order to investigate the influence of different linkers on the MOF porosity (Figure 5a,b). The N_2 sorption isotherms indicate that the porosity of PCN-700 is well-maintained and precisely controlled during linker installation. The lengths of the installed linkers along the *a*-axis directly correlate to the MOF porosity, as proven by the total N_2 uptake. The channel size along the *a*-axis can be readily tuned by the size of installed linkers. The length of FA (4.95 Å) is shorter than the distance between adjacent Zr_6 clusters in pristine PCN-700 (6.98 Å) so that the installation of FA squeezes the structure. The installation of the BDC linker did not change the unit cell parameter by a large amount, whereas the NDC and BPDC open up the MOF cavity along the *a*-axis. With gradually increased length of linear linkers, the N_2 total uptake increased from 328 (compound **1**) to 638 cm^3g^{-1} (compound **4**). The linker installation affects the MOF porosity in two ways. On one hand, the installed linker occupies the free space inside the MOF cavity, which would decrease the MOF porosity. On the other hand, a linker with proper length can open up the MOF cavity along the *a* direction, which results in a dramatic swell in unit cell volume and therefore increases porosity. For example, the N_2 uptake of PCN-700 is enhanced by 33.4% after BPDC installation; meanwhile, the cell volume increased by 17.4%. The installation of TPDC and BDDC does not further increase the pore volume as they occupy different cavities compared with BPDC. Therefore, the installation of BPDC resulted in the largest enhancement of porosity.

The pore environment of PCN-700 can be decorated by functionalized linkers. The H_2 adsorption isotherms illustrate the beneficial effect of different functional groups on the pore environments and therefore the MOF properties. For example,

DOI: 10.1021/jacs.6b04501
J. Am. Chem. Soc. 2016, 138, 8912−8919

the replacement of methyl groups with nitro groups on the primary linker of PCN-700 increases its H_2 adsorption capacities by 47% (Figures 5c and S17). Systematic variation of the pore volume and decoration of pore environment have a synergistic effect on the adsorption behavior. A certain combination of linkers (PCN-700-$(NO_2)_2$-BPDC) displays increases in their H_2 adsorption capacities of 57% compared to that of the parent framework (PCN-700) (Figures 5d and S19).

Size-Selective Catalytic System Built through Linker Installation. PCN-700 demonstrates a nearly ideal platform for systematic modulation of pore volume and pore environment by judicious selection of linkers. This leads to a highly tunable multifunctional MOF system that is capable of complex functional behavior. Herein, we show that a size-selective catalytic system for the aerobic alcohol oxidation reaction can be built in PCN-700 through the sequential installation of BPYDC(Cu) (Figure 6b) and TPDC-R_2 (R = Me, Ph, or Hex, Figure 6c). The BPYDC(Cu) moiety acts as the catalytic active center, while the TPDC-R_2 with different substituents controls the selectivity of substrates (Figure 6a). Two components within the cavity of PCN-700 work synergistically as a size-selective catalyst for the aerobic alcohol oxidation (Scheme 2).

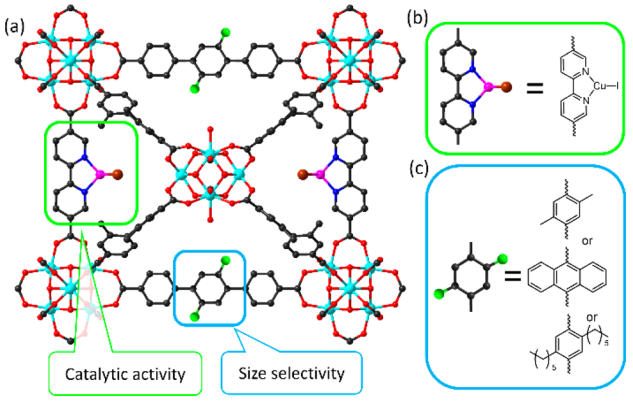

Figure 6. (a) Size-selective catalytic system for aerobic alcohol oxidation reaction built in PCN-700 through linker installation. (b,c) Structure of catalytic center and size-selective moiety. Coordinated CH_3CN on the Cu is removed for clarity.

Scheme 2. Aerobic Oxidation of Alcohol Using BPYDC(Cu)-Functionalized PCN-700

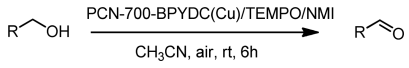

Conversion of alcohols to aldehydes and ketones is among the most important and widely used class of oxidation reactions in organic chemical synthesis and industry.[18] The aerobic alcohol oxidation promoted by the (bpy)Cu/TEMPO catalyst system (bpy = 2,2′-bipyridine, TEMPO = 2,2,6,6-tetramethylpiperidine-*N*-oxyl) catalyst has been reported in the literature as a particularly versatile and effective method.[19] The immobilization of the (bpy)Cu catalyst in MOFs offers several advantages over the homogeneous systems, such as easy catalyst separation and recovery, regeneration, and handling. In addition, the well-defined pores of MOF catalysts may favor shape and size selectivity, which is difficult to realize in homogeneous catalysts. For catalytic applications, PCN-700 provides unique advantages because its pore size can be tuned by the installation of different linkers, giving rise to a controllable size-selective catalytic system. This incentivizes us to immobilize the (bpy)Cu catalyst in PCN-700 and, at the same time, tune the size selectivity via linker installation.

The PCN-700-BPYDC(Cu)-TPDC system was assembled via stepwise linker installation and metalation. First, the BPYDC and TPDC-R_2 were sequentially installed by treating PCN-700 crystals with solutions of BPYDC and TPDC-R_2 in DMF at 75 °C. PCN-700-BPYDC-TPDC-R_2 bears open bipyridine sites that readily react with CuI in acetonitrile to form the metalated framework. The single-crystal structure of PCN-700-BPYDC(Cu)-TPDC-R_2 clearly shows the existence and position of BPYDC(Cu) and TPDC-R_2 components within the framework. The coordination environment of Cu^+ is clearly determined in the single-crystal structure, which provides direct structure evidence of the catalytic center. According to the crystal structure, the Cu^+ center is chelated by a bipyridine group and further coordinated with a N from acetonitrile and an I^- ion as a counterion. PCN-700 is an inherent crystalline platform allowing for the metalations to occur quantitatively without appreciable loss of crystallinity, thereby enabling examination of the catalytic center by single-crystal X-ray diffraction. As shown in Figure S30, the Cu^+ center is arranged around the 1D channel along the *c*-axis, whereas the TPDC-R_2 controls the accessibility of the Cu^+ center by partially blocking the channels. Therefore, the size selectivity of the whole material can be tuned by changing the size of substituents on the TPDC-R_2 linker. To evaluate our hypothesis, the TPDC-R_2 linker was functionalized by methyl groups, phenyl groups, and hexyl groups, which is expected to result in different selectivity toward the substrates.

The catalytic performance of the PCN-700-BPYDC(Cu)-TPDC-R_2 system in the oxidation of various alcohols with different molecular sizes were evaluated. As shown in Figure 7 and Table S4, alcohols were converted to corresponding aldehyde in good yields and high selectivity for homogeneous reference, regardless of the molecular size. The yield of benzaldehyde catalyzed by PCN-700-BPYDC(Cu) is as high as

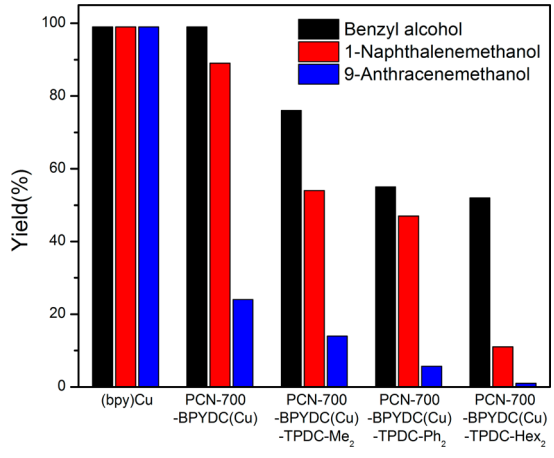

Figure 7. Size-selective alcohol aerobic oxidation using PCN-700 installed with different linkers. Reaction conditions: alcohol (0.5 mmol), catalyst (0.005 mmol based on Cu), TEMPO (0.05 mmol), *N*-methylimidazole (0.05 mmol), CH_3CN (5.0 mL), ambient air, room temperature, 6 h. Yields were determined by ^1H NMR analysis and calculated based on the ratios of product/(product + starting material).

DOI: 10.1021/jacs.6b04501
J. Am. Chem. Soc. 2016, 138, 8912−8919

the homogeneous reference, suggesting the high accessibility and activity of the (bpy)Cu moiety within the MOF cavity. Indeed, the size of benzyl alcohol (~4.3 Å) is much smaller than the channel size of PCN-700-BPYDC(Cu) (~14 Å), which allows for efficient diffusion of the substrate (Figure S30). The increase of the aromatic rings on alcohol decreases yields of the corresponding aldehydes under the same condition, showing a clear size selectivity. 9-Anthracenemethanol shows a relative low yield (24%) catalyzed by PCN-700-BPYDC(Cu), perhaps resulting from the large molecular size (9.2 Å) which limits the diffusion rate of substrate and the accessibility of catalytic centers.

By installation of TPDC with different functional groups into PCN-700-BPYDC(Cu), the size selectivity can be fine-tuned. The TPDC partially blocks the channel along the *c*-axis, which affects the diffusion of substrate as well as the accessibility of the Cu^+ center (Figure S30). By increasing the size of substituents on the TPDC linker, the yields of the alcohol conversion are dramatically decreased, especially for bulky substrates (Figure 7 and Table S4). With TPDC-Hex_2 installed, the 9-anthracene alcohol is almost excluded by the small MOF cavity, which explains the lowest yield (<1%). The guest-selective alcohol oxidation reaction suggested that the catalytic reaction occurred exclusively in the MOF cavity, whereas the external surface of the MOF crystal was only responsible for very limited conversion of alcohols. Based on the experimental result and literature, a simplified mechanism is proposed for the aerobic alcohol oxidation reaction catalyzed by PCN-700-BPYDC(Cu), which is shown in Scheme S2. To evaluate the recyclability, the PCN-700-BPYDC(Cu) catalyst was simply separated from the mixture at the end of the reaction by centrifuge and reused for the next reaction. The catalytic activity was well-maintained after three cycles (Table S5). PCN-700 can be functionalized with various catalysts by judicious selection of chelating linkers and metal precursor, allowing the development of heterogeneous catalysts with an unprecedented degree of control. The PCN-700 system also serves as an inherent crystalline platform, possibly facilitating the observation of a catalytic center and reaction intermediates by single-crystal X-ray diffraction to gather fundamental insight into metal-catalyzed reactions.

CONCLUSIONS

In summary, we present a comprehensive study on the linker installation method. First, kinetic analysis was adopted to construct a MOF with inherent missing linker sites, namely, PCN-700. Twelve linkers with different substituents were designed to study the size effect of functional groups on the linkers. Guided by the geometrical analysis, linkers with different lengths and combinations thereof were sequentially installed into a parent PCN-700, giving rise to 11 new MOFs, and each bearing up to three different functional groups in predefined positions. The pore environments of the PCN-700 system were engineered by tuning the sizes and functionalities of installed linkers. Systematic variation of the pore volume and decoration of pore environment resulted in synergistic effects including an enhancement of H_2 uptake to 57%. Besides, a size-selective catalytic system for aerobic alcohol oxidation was built in PCN-700 through linker installation, which showed high activity and tunable size selectivity. These results highlight the unique potential of the linker installation method to decorate the pore environment of the MOF with multiple functional groups in a highly designed manner. In light of the ubiquity of Zr-MOFs with coordinately unsaturated Zr_6 clusters, we believe that linker installation is a versatile strategy to synthesize stable MOFs with unprecedented multifunctionality.

ASSOCIATED CONTENT

Supporting Information

The Supporting Information is available free of charge on the ACS Publications website at DOI: 10.1021/jacs.6b04501.

Experimental details, figures, tables and crystallographic data (PDF)
Linker installation (CIF)
Linker modification (CIF)

AUTHOR INFORMATION

Corresponding Author

*zhou@chem.tamu.edu

Author Contributions

⊥S.Y. and Y.-P.C. contributed equally.

Notes

The authors declare no competing financial interest.

ACKNOWLEDGMENTS

The gas adsorption−desorption studies of this research was supported by the Center for Gas Separations Relevant to Clean Energy Technologies, an Energy Frontier Research Center funded by the U.S. Department of Energy, Office of Science, Office of Basic Energy Sciences under Award Number DE-SC0001015. Structural analyses were supported as part of the Hydrogen and Fuel Cell Program under Award Number DE-EE-0007049. S.Y. also acknowledges the Texas A&M Energy Institute Graduate Fellowship funded by ConocoPhillips and Dow Chemical Graduate Fellowship. We thank Mr. Mathieu Bosch for his proofreading and feedback.

REFERENCES

(1) (a) Zhou, H. C.; Long, J. R.; Yaghi, O. M. *Chem. Rev.* **2012**, *112*, 673. (b) Li, H.; Eddaoudi, M.; O'Keeffe, M.; Yaghi, O. M. *Nature* **1999**, *402*, 276. (c) Furukawa, H.; Cordova, K. E.; O'Keeffe, M.; Yaghi, O. M. *Science* **2013**, *341*, 1230444.

(2) (a) Yaghi, O. M.; O'Keeffe, M.; Ockwig, N. W.; Chae, H. K.; Eddaoudi, M.; Kim, J. *Nature* **2003**, *423*, 705. (b) Li, M.; Li, D.; O'Keeffe, M.; Yaghi, O. M. *Chem. Rev.* **2014**, *114*, 1343. (c) Furukawa, H.; Ko, N.; Go, Y. B.; Aratani, N.; Choi, S. B.; Choi, E.; Yazaydin, A. O.; Snurr, R. Q.; O'Keeffe, M.; Kim, J.; Yaghi, O. M. *Science* **2010**, *329*, 424. (d) Fukushima, T.; Horike, S.; Inubushi, Y.; Nakagawa, K.; Kubota, Y.; Takata, M.; Kitagawa, S. *Angew. Chem., Int. Ed.* **2010**, *49*, 4820. (e) Doonan, C. J.; Morris, W.; Furukawa, H.; Yaghi, O. M. *J. Am. Chem. Soc.* **2009**, *131*, 9492. (f) Dybtsev, D. N.; Chun, H.; Kim, K. *Angew. Chem., Int. Ed.* **2004**, *43*, 5033.

(3) (a) Makal, T. A.; Li, J.-R.; Lu, W.; Zhou, H.-C. *Chem. Soc. Rev.* **2012**, *41*, 7761. (b) Ma, L.; Abney, C.; Lin, W. *Chem. Soc. Rev.* **2009**, *38*, 1248. (c) Li, J. R.; Kuppler, R. J.; Zhou, H. C. *Chem. Soc. Rev.* **2009**, *38*, 1477. (d) Sumida, K.; Rogow, D. L.; Mason, J. A.; McDonald, T. M.; Bloch, E. D.; Herm, Z. R.; Bae, T. H.; Long, J. R. *Chem. Rev.* **2012**, *112*, 724. (e) Suh, M. P.; Park, H. J.; Prasad, T. K.; Lim, D. W. *Chem. Rev.* **2012**, *112*, 782. (f) Li, J.-R.; Sculley, J.; Zhou, H.-C. *Chem. Rev.* **2012**, *112*, 869.

(4) (a) Cavka, J. H.; Jakobsen, S.; Olsbye, U.; Guillou, N.; Lamberti, C.; Bordiga, S.; Lillerud, K. P. *J. Am. Chem. Soc.* **2008**, *130*, 13850. (b) Bai, Y.; Dou, Y.; Xie, L.-H.; Rutledge, W.; Li, J.-R.; Zhou, H.-C. *Chem. Soc. Rev.* **2016**, *45*, 2327. (c) Feng, D.; Gu, Z.-Y.; Li, J.-R.; Jiang, H.-L.; Wei, Z.; Zhou, H.-C. *Angew. Chem., Int. Ed.* **2012**, *51*, 10307. (d) Lin, Q.; Bu, X.; Kong, A.; Mao, C.; Zhao, X.; Bu, F.; Feng, P. *J. Am. Chem. Soc.* **2015**, *137*, 2235. (e) Liu, T.-F.; Feng, D.; Chen, Y.-P.; Zou,

DOI: 10.1021/jacs.6b04501
J. Am. Chem. Soc. 2016, 138, 8912−8919

L.; Bosch, M.; Yuan, S.; Wei, Z.; Fordham, S.; Wang, K.; Zhou, H.-C. *J. Am. Chem. Soc.* **2015**, *137*, 413. (f) Morris, W.; Volosskiy, B.; Demir, S.; Gándara, F.; McGrier, P. L.; Furukawa, H.; Cascio, D.; Stoddart, J. F.; Yaghi, O. M. *Inorg. Chem.* **2012**, *51*, 6443. (g) Schaate, A.; Roy, P.; Preuße, T.; Lohmeier, S. J.; Godt, A.; Behrens, P. *Chem. - Eur. J.* **2011**, *17*, 9320. (h) Wu, H.; Chua, Y. S.; Krungleviciute, V.; Tyagi, M.; Chen, P.; Yildirim, T.; Zhou, W. *J. Am. Chem. Soc.* **2013**, *135*, 10525. (i) Mondloch, J. E.; Bury, W.; Fairen-Jimenez, D.; Kwon, S.; DeMarco, E. J.; Weston, M. H.; Sarjeant, A. A.; Nguyen, S. T.; Stair, P. C.; Snurr, R. Q.; Farha, O. K.; Hupp, J. T. *J. Am. Chem. Soc.* **2013**, *135*, 10294. (j) Yuan, S.; Chen, Y.-P.; Qin, J.; Lu, W.; Wang, X.; Zhang, Q.; Bosch, M.; Liu, T.-F.; Lian, X.; Zhou, H.-C. *Angew. Chem., Int. Ed.* **2015**, *54*, 14696. (k) Cliffe, M. J.; Wan, W.; Zou, X.; Chater, P. A.; Kleppe, A. K.; Tucker, M. G.; Wilhelm, H.; Funnell, N. P.; Coudert, F.-X.; Goodwin, A. L. *Nat. Commun.* **2014**, *5*, 4176.

(5) (a) Furukawa, H.; Gándara, F.; Zhang, Y.-B.; Jiang, J.; Queen, W. L.; Hudson, M. R.; Yaghi, O. M. *J. Am. Chem. Soc.* **2014**, *136*, 4369. (b) Katz, M. J.; Brown, Z. J.; Colon, Y. J.; Siu, P. W.; Scheidt, K. A.; Snurr, R. Q.; Hupp, J. T.; Farha, O. K. *Chem. Commun.* **2013**, *49*, 9449. (c) Schaate, A.; Roy, P.; Godt, A.; Lippke, J.; Waltz, F.; Wiebcke, M.; Behrens, P. *Chem. - Eur. J.* **2011**, *17*, 6643.

(6) Yamada, T.; Kitagawa, H. *J. Am. Chem. Soc.* **2009**, *131*, 6312.

(7) (a) Tanabe, K. K.; Cohen, S. M. *Chem. Soc. Rev.* **2011**, *40*, 498. (b) Kim, M.; Cohen, S. M. *CrystEngComm* **2012**, *14*, 4096. (c) Nickerl, G.; Senkovska, I.; Kaskel, S. *Chem. Commun.* **2015**, *51*, 2280. (d) Kandiah, M.; Usseglio, S.; Svelle, S.; Olsbye, U.; Lillerud, K. P.; Tilset, M. *J. Mater. Chem.* **2010**, *20*, 9848. (e) Wang, T. C.; Vermeulen, N. A.; Kim, I. S.; Martinson, A. B. F.; Stoddart, J. F.; Hupp, J. T.; Farha, O. K. *Nat. Protoc.* **2016**, *11*, 149. (f) Deria, P.; Mondloch, J. E.; Karagiaridi, O.; Bury, W.; Hupp, J. T.; Farha, O. K. *Chem. Soc. Rev.* **2014**, *43*, 5896.

(8) Pullen, S.; Fei, H.; Orthaber, A.; Cohen, S. M.; Ott, S. *J. Am. Chem. Soc.* **2013**, *135*, 16997.

(9) (a) Deria, P.; Chung, Y. G.; Snurr, R. Q.; Hupp, J. T.; Farha, O. K. *Chem. Sci.* **2015**, *6*, 5172. (b) Deria, P.; Bury, W.; Hod, I.; Kung, C.-W.; Karagiaridi, O.; Hupp, J. T.; Farha, O. K. *Inorg. Chem.* **2015**, *54*, 2185. (c) Deria, P.; Bury, W.; Hupp, J. T.; Farha, O. K. *Chem. Commun.* **2014**, *50*, 1965. (d) Deria, P.; Mondloch, J. E.; Tylianakis, E.; Ghosh, P.; Bury, W.; Snurr, R. Q.; Hupp, J. T.; Farha, O. K. *J. Am. Chem. Soc.* **2013**, *135*, 16801.

(10) Jiang, H.-L.; Feng, D.; Liu, T.-F.; Li, J.-R.; Zhou, H.-C. *J. Am. Chem. Soc.* **2012**, *134*, 14690.

(11) (a) Chevreau, H.; Devic, T.; Salles, F.; Maurin, G.; Stock, N.; Serre, C. *Angew. Chem., Int. Ed.* **2013**, *52*, 5056. (b) Burrows, A. D. *CrystEngComm* **2011**, *13*, 3623. (c) Kong, X.; Deng, H.; Yan, F.; Kim, J.; Swisher, J. A.; Smit, B.; Yaghi, O. M.; Reimer, J. A. *Science* **2013**, *341*, 882. (d) Deng, H.; Doonan, C. J.; Furukawa, H.; Ferreira, R. B.; Towne, J.; Knobler, C. B.; Wang, B.; Yaghi, O. M. *Science* **2010**, *327*, 846. (e) Tu, B.; Pang, Q.; Ning, E.; Yan, W.; Qi, Y.; Wu, D.; Li, Q. *J. Am. Chem. Soc.* **2015**, *137*, 13456. (f) Zhao, X.; Bu, X.; Zhai, Q.-G.; Tran, H.; Feng, P. *J. Am. Chem. Soc.* **2015**, *137*, 1396. (g) Müller, P.; Wisser, F. M.; Bon, V.; Grünker, R.; Senkovska, I.; Kaskel, S. *Chem. Mater.* **2015**, *27*, 2460.

(12) (a) Liu, L.; Konstas, K.; Hill, M. R.; Telfer, S. G. *J. Am. Chem. Soc.* **2013**, *135*, 17731. (b) Liu, L.; Telfer, S. G. *J. Am. Chem. Soc.* **2015**, *137*, 3901.

(13) Yuan, S.; Lu, W.; Chen, Y.-P.; Zhang, Q.; Liu, T.-F.; Feng, D.; Wang, X.; Qin, J.; Zhou, H.-C. *J. Am. Chem. Soc.* **2015**, *137*, 3177.

(14) Gutov, O. V.; Hevia, M. G.; Escudero-Adán, E. C.; Shafir, A. *Inorg. Chem.* **2015**, *54*, 8396.

(15) (a) Eddaoudi, M.; Kim, J.; O'Keeffe, M.; Yaghi, O. M. *J. Am. Chem. Soc.* **2002**, *124*, 376. (b) Eddaoudi, M.; Kim, J.; Vodak, D.; Sudik, A.; Wachter, J.; O'Keeffe, M.; Yaghi, O. M. *Proc. Natl. Acad. Sci. U. S. A.* **2002**, *99*, 4900. (c) Zhao, D.; Timmons, D. J.; Yuan, D. Q.; Zhou, H. C. *Acc. Chem. Res.* **2011**, *44*, 123. (d) Chen, Y.-P.; Liu, T.-F.; Fordham, S.; Zhou, H.-C. *Acta Crystallogr., Sect. B: Struct. Sci., Cryst. Eng. Mater.* **2015**, *71*, 613. (e) Wang, X.; Lu, W.; Gu, Z.-Y.; Wei, Z.; Zhou, H.-C. *Chem. Commun.* **2016**, *52*, 1926. (f) Delgado-Friedrichs, O.; O'Keeffe, M.; Yaghi, O. M. *Acta Crystallogr., Sect. A: Found. Crystallogr.* **2006**, *62*, 350.

(16) Mondloch, J. E.; Katz, M. J.; Planas, N.; Semrouni, D.; Gagliardi, L.; Hupp, J. T.; Farha, O. K. *Chem. Commun.* **2014**, *50*, 8944.

(17) Blatov, V. A. T. P. Multipurpose crystallochemical analysis with the program package TOPOS. In *Commission on Crystallographic Computing*, 2006; http://www.iucr.org/__data/assets/pdf_file/0004/6358/iucrcompcomm_nov2006.pdf.

(18) (a) Corey, E. J.; Suggs, J. W. *Tetrahedron Lett.* **1975**, *16*, 2647. (b) Ladbury, J. W.; Cullis, C. F. *Chem. Rev.* **1958**, *58*, 403. (c) Dhakshinamoorthy, A.; Alvaro, M.; Garcia, H. *Catal. Sci. Technol.* **2011**, *1*, 856. (d) Yuan, S.; Liu, T.-F.; Feng, D.; Tian, J.; Wang, K.; Qin, J.; Zhang, Q.; Chen, Y.-P.; Bosch, M.; Zou, L.; Teat, S. J.; Dalgarno, S. J.; Zhou, H.-C. *Chem. Sci.* **2015**, *6*, 3926.

(19) (a) Hoover, J. M.; Ryland, B. L.; Stahl, S. S. *J. Am. Chem. Soc.* **2013**, *135*, 2357. (b) Hoover, J. M.; Stahl, S. S. *J. Am. Chem. Soc.* **2011**, *133*, 16901.

DOI: 10.1021/jacs.6b04501
J. Am. Chem. Soc. 2016, 138, 8912−8919